American Journal of Transplantation 2016; 16: 468–483
Wiley Periodicals Inc.



doi: 10.1111/ajt.13537

# A Distinct Subpopulation of Bone Marrow Mesenchymal Stem Cells, Muse Cells, Directly Commit to the Replacement of Liver Components

**H. Katagiri[1,2], Y. Kushida[3], M. Nojima[4], Y. Kuroda[3], S. Wakao[4], K. Ishida[1,2], F. Endo[1,2], K. Kume[1,2,5,6], T. Takahara[2], H. Nitta[2], H. Tsuda[7,†], M. Dezawa[3,4] and S. S. Nishizuka[1,2,5,6,8,9,*]**

[1]*Molecular Therapeutics Laboratory, Iwate Medical University School of Medicine, Morioka, Japan*
[2]*Department of Surgery, Iwate Medical University School of Medicine, Morioka, Japan*
[3]*Department of Anatomy and Anthropology, Tohoku University Graduate School of Medicine, Sendai, Japan*
[4]*Department of Stem Cell Biology and Histology, Tohoku University Graduate School of Medicine, Sendai, Japan*
[5]*Institute for Biomedical Sciences, Iwate Medical University, Yahaba, Japan*
[6]*Medical Innovation by Advanced Science and Technology Program, Iwate Medical University, Morioka, Japan*
[7]*Diagnostic Pathology Section, Clinical Laboratory Division, National Cancer Center Hospital, Tokyo, Japan*
[8]*Department of Surgery, Iwate Medical University School of Dentistry, Morioka, Japan*
[9]*Iwate Tohoku Medical Megabank Organization, Iwate Medical University, Yahaba, Japan*
[*]*Corresponding author: Satoshi S. Nishizuka, snishizu@iwate-med.ac.jp*
[†]*Present address: Department of Basic Pathology, National Defense Medical College, Tokorozawa, Japan*

**Genotyping graft livers by short tandem repeats after human living-donor liver transplantation (n = 20) revealed the presence of recipient or chimeric genotype cases in hepatocytes (6 of 17, 35.3%), sinusoidal cells (18 of 18, 100%), cholangiocytes (15 of 17, 88.2%) and cells in the periportal areas (7 of 8, 87.5%), suggesting extrahepatic cell involvement in liver regeneration. Regarding extrahepatic origin, bone marrow mesenchymal stem cells (BM-MSCs) have been suggested to contribute to liver regeneration but compose a heterogeneous population. We focused on a more specific subpopulation (1–2% of BM-MSCs), called multilineage-differentiating stress-enduring (Muse) cells, for their ability to differentiate into liver-lineage cells and repair tissue. We generated a physical partial hepatectomy model in immunodeficient mice and injected green fluorescent protein (GFP)-labeled human BM-MSC Muse cells intravenously (n = 20). Immunohistochemistry, fluorescence *in situ* hybridization and species-specific polymerase chain reaction revealed that they integrated into regenerating areas and expressed liver progenitor markers during the early phase and then differentiated spontaneously into major liver components, including hepatocytes (≈74.3% of GFP-positive integrated Muse cells), cholangiocytes (≈17.7%), sinusoidal endothelial cells (≈2.0%), and Kupffer cells (≈6.0%). In contrast, the remaining cells in the BM-MSCs were not detected in the liver for up to 4 weeks. These results suggest that Muse cells are the predominant population of BM-MSCs that are capable of replacing major liver components during liver regeneration.**

**Abbreviations: AFP, α-fetoprotein; APC, allophycocyanin; BM, bone marrow; BM-MSC, bone marrow mesenchymal stem cell; C, caudate lobe; D, donor; DAPI, 4′,6-diamidino-2-phenylindole; FACS, fluorescence-activated cell sorting; FISH, fluorescence *in situ* hybridization; GFP, green fluorescent protein; h, human; h-BM-MSC, human bone marrow mesenchymal stem cell; HepPar-1, hepatocyte paraffin 1; IHC, immunohistochemistry; LDLT, living donor liver transplantation; M, median lobe; MSCs, mesenchymal stem cells; Muse, multilineage-differentiating stress-enduring; NA, necrotic area; NI, not informative; PBS, phosphate-buffered saline; PBMC, peripheral blood mononuclear cells; PPHx, physical partial hepatectomy; PTGER2, prostaglandin E receptor 2; PV, portal vein; R, recipient; SCID, severe combined immunodeficiency; SEC, sinusoidal endothelial cells; SSEA-3, stage-specific embryonic antigen-3; STR, single tandem repeat; W, weeks**

**Received 03 November 2014, revised 23 August 2015 and accepted for publication 06 September 2015**

## Introduction

Among multipotent cells of extrahepatic origin, bone marrow mesenchymal stem cells (BM-MSCs) have been postulated to have the potential to contribute to liver regeneration (1,2). BM-MSCs are heterogeneous cell populations because they are generally collected solely as adherent cells from bone marrow (BM) aspirates (3,4). In fact, standard mesenchymal markers are expressed in the majority of BM-MSCs, although the expression ratios are not always consistent because they generally depend on

methodological factors. Moreover, BM-MSCs engrafted into damaged liver often include cells with markers that are irrelevant to mesenchymal stem cells (MSCs) (5).

Among possible extrahepatic progenitor cells for liver regeneration, BM-MSCs have attracted attention because they (a) exhibit plasticity to differentiate into mesenchymal-to-endodermal-lineage cells that express hepatic markers *in vitro* (6), (b) are suggested to include a very small portion of cells that integrate into the liver when transplanted *in vivo* (7) and (c) secrete factors associated with hepatocyte differentiation (8). Consequently, identification of the distinct subpopulation in BM-MSCs that is responsible for differentiating into the liver components would support a rationale for the involvement of BM-MSCs in liver regeneration.

In the present study, we focused on a recently reported, unique stem cell population in adult human BM-MSCs (h-BM-MSCs), namely multilineage-differentiating stress-enduring (Muse) cells (6). Muse cells compose ≈1% of human BM-MSCs and, in human BM aspirates, represent ≈0.03% of BM-mononucleated cells (9). Muse cells can be isolated as cells positive for stage-specific embryonic antigen-3 (SSEA-3$^{+}$), which is a well-known marker for undifferentiated human embryonic stem cells, in addition to expressing other pluripotency markers, including Oct3/4, Sox2 and Nanog and general MSC markers, such as CD105 and CD90 (6). Individual Muse cells can differentiate into cells of all three germ layers (endoderm, mesoderm and ectoderm) and can self-renew, but they do not have tumorigenic proliferative activity (6). Spontaneous differentiation of cells positive for cytokeratin-7 (CK7), a marker of endodermal lineage biliary cells, was demonstrated when a single Muse cell was expanded on gelatin (6). Muse cells treated in culture with insulin-transferrin-selenium, dexamethasone, hepatocyte growth factor and fibroblast growth factor 4 differentiate into cells positive for α-fetoprotein (AFP) and/or albumin (9). Importantly, naive Muse cells injected either locally or into the blood stream of animal models of tissue damage integrated into the damaged sites, spontaneously differentiated into cells that were compatible with that microenvironment and participated in tissue repair (6,10–12).

In this study, we demonstrated that extrahepatic recipient cells are detectable in donor-derived liver as a liver component in human living donor liver transplantation (LDLT). This observation led us to attempt to identify a specific cell population from extrahepatic origin that may contribute to liver regeneration. To confirm this in an animal model, we designed a physical partial hepatectomy (PPHx) model in immunodeficient mice that mimics a human hepatectomy in LDLT donors and then transplanted GFP-labeled human BM-MSC–derived Muse cells into the blood stream to trace their integration into the liver and differentiation *in vivo* into a liver component (13,14). We also examined whether the remaining cells of the human GFP-labeled BM-MSC population, namely, non-Muse cells, contributed to liver regeneration. We present a plausible process for liver regeneration in which Muse cells are the predominant cell population that directly contributes to replacement of the lost liver components during liver regeneration, and the contribution of non-Muse cells is extremely limited.

## Materials and Methods

### *Human participants*

Twenty recipient–donor pairs who underwent LDLT (Figure S1) from January 2007 to February 2011 in the Department of Surgery at Iwate Medical University Hospital in Morioka, Japan were analyzed. The samples included 20 removed livers from the recipients, 20 zero-point biopsies from the donors and 56 needle biopsies of the grafts. A zero-point biopsy is used to test the quality of the donor liver before transplantation. Of the 20 LDLT recipients, 19 were adults and one was a child. The graft biopsies used in the present study were taken at various time points between 1 and 24 months after LDLT and were reviewed retrospectively. The study protocol was reviewed and approved by the ethics committee of Iwate Medical University School of Medicine (HG H23-13). Informed consent was obtained from all donors and recipients, according to institutional review board guidelines. Reagents and controls used for LDLT specimens are shown in Tables S1 and S2 and Figure S2.

### *Isolation of Muse and non-Muse cells*

The h-BM-MSC population (item C-12974; Lonza, Basel, Switzerland) was used as the source of Muse and non-Muse cells. The h-BM-MSCs were labeled with GFP-labeled lentivirus, as reported previously (6,15). Examination using fluorescence microscopy confirmed that ≈50% of the h-BM-MSCs were GFP positive. Cells were maintained in α-Minimum Essential Media containing 10% fetal bovine serum and 0.1 mg/mL kanamycin in a humidified cell incubator at 37°C with 5% $CO_2$. Cells from the fifth to 10th subcultures were used in this study (6,9). Fluorescence-activated cell sorting (FACS) was used to isolate Muse and non-Muse cells from GFP-labeled h-BM-MSCs. Cells were first incubated with rat anti–SSEA-3 IgM antibody (clone MC-631; Millipore, Billerica, MA) and further incubated with an allophycocyanin-conjugated goat antirat IgM antibody (Jackson ImmunoResearch, West Grove, PA). Data collection and analysis were performed using FACSAria and DIVA software (BD Biosciences, San Jose, CA). Muse cells were collected as the GFP$^{+}$/SSEA-3$^{+}$ cell fraction, and non-Muse cells were defined as the GFP$^{+}$/SSEA-3$^{-}$ fraction.

### *Mice*

All animal experiments in this study were approved by both the Iwate Medical University Ethics Committee for Animal Experiment Regulation (23-056) and Regulations for Animal Experiments and Related Activities at Tohoku University (2012-459). A total of 42 female severe combined immunodeficiency (SCID) C.B-17/ICR-SCID/SCID mice (CLEA Japan Inc., Tokyo, Japan) aged 8 weeks were used for the experiments. The following number of mice were used for the respective experiments to determine cellular reactions at 1, 2, 3, and 4 days after PPHx (n = 3 per group) and at 2 days and 1, 2, and 4 weeks after PPHx, followed by either transplantation of Muse cells (n = 5 per group) or non-Muse cells (n = 5 per group).

### *Transplantation of Muse and non-Muse cells*

The method for isolation of human Muse and non-Muse cells from h-BM-MSCs is described in the Supporting Information. A human Muse cell population was isolated from GFP-labeled h-BM-MSCs using the

SSEA-3$^+$ cell population (6,9). Approximately 1% of the GFP-labeled h-BM-MSCs were SSEA-3$^+$, which is consistent with a previous report (6). GFP-labeled h-BM-MCSs were separated into Muse cell (GFP$^+$/SSEA-3$^+$) and non-Muse cell (GFP$^+$/SSEA-3$^-$) populations by FACS. After creating the PPHx model using a harmonic scalpel, either the Muse or non-Muse cell population at a concentration of $1.0 \times 10^4$ cells in 400 μL phosphate-buffered saline (PBS) was injected into the tail vein of SCID mice 24 h after PPHx. The control group received a tail vein injection of the same volume of PBS. Mice transplanted with either Muse or non-Muse cells were fixed at 2 days, 1 week, 2 weeks and 4 weeks (n = 5 per group) after transplantation for immunohistochemical analysis (Table S2).

## Results

### *Molecular genetics of LDLT allografts*

The clinical characteristics of the LDLT grafts are shown in Table S3. All genetic assessments were performed with DNA/RNA from formalin-fixed paraffin-embedded needle biopsies taken far from the damaged area of the graft after partial hepatectomy. The prevalence of the recipient single tandem repeat (STR) genotype (chimeric or recipient genotype only) by cell type isolated with laser microdissection was as follows: hepatocytes in 35.3% of patients (6 of 17), sinusoidal cells in 100% of patients (18 of 18), cholangiocytes in 88.2% of patients (15 of 17) and periportal area cells in 87.5% of patients (7 of 8) (Table 1 and Figures 1A–D and S3).

To rule out the presence of hematopoietic and nonepithelial cells in microdissected samples, reverse transcription–polymerase chain reaction was performed using CD45 (hematopoietic marker) (16) and vimentin (nonepithelial marker) (17) as markers. The chimeric genotype was partially due to recipient blood cells in sinusoidal cells, but the recipient blood cells did not seem to contribute substantially to the chimeric genotype in other cell types (Figure 1E).

For immunohistochemical analysis, the entire sections of needle biopsy specimens (n = 8) were subject to bile duct count. The majority of cells composing bile duct–like structures, particularly those in the periportal area, was found to express liver progenitor protein markers CK19 and AFP (Figure 1F). One to five periportal regions were present in each specimen, and a total of 27 periportal regions were evaluated. An average of 93.4 CK19$^+$ cells per specimen were observed, of which 3.5 cells were CK19$^+$/AFP$^+$ (3.7%).

The prevalence of cells with recipient genotype in LDLT was assessed by fluorescent *in situ* hybridization (FISH) of Y chromosomes among cell types identified by immunohistochemistry in three sex-mismatched cases (Figure 1G and Table S4). Polyploid hepatocytes were occasionally seen at 17.0% (15 of 88 hepatocytes) in patient 4, 8.6% (6 of 70) in patient 18 and 12.5% (5 of 40) in patient 19. All polyploid hepatocytes possessed only X chromosomes. The average frequency of the Y chromosome (i.e. recipient origin) of each cell fraction was extremely small in hepatocytes (average 0.4%). Cholangiocytes were occasionally chimeric (16.1%), whereas cells showed more frequent chimerism in the periportal (36.4%) and sinusoidal zone (36.7%), most likely due to proliferation of recipient blood cells. We also compared ''allele frequency'' by quantification of STR histograms and Y chromosome frequency by FISH (Table S5). Although analyzable STR markers and biopsy sections were limited, the frequency of sinusoidal cells and cholangiocytes were comparable.

Taken together, these data suggest (a) that a substantial fraction (>35%) of cells in the sinusoid and periportal are of recipient origin; (b) that cells from an extrahepatic origin are preferably integrated as cholangiocytes; and (c) that direct integration of extrahepatic cells as hepatocytes is not a rare event (35.3%) in the LDLT patient population, but the frequency of extrahepatic cells in individual grafted livers at the tissue level from the biopsy is very small (0.4%).

### *Isolation of BM-MSC-derived Muse and non-Muse cells*

The genotyping results of LDLT led us to examine the potential of Muse cells contributing to liver regeneration in PPHx. GFP-labeled human Muse cells (SSEA-3$^+$) and non-Muse cells (SSEA-3$^-$) were isolated from GFP-labeled h-BM-MSCs. Approximately 1% of the h-BM-MSCs were SSEA-3$^+$, which was consistent with a previous report (Figure 2A and B) (6).

**Table 1:** The number of cases with recipient-derived or chimeric genotypes of different cell fractions from biopsy specimens of the LDLT grafts

| | Hepatocyte | Sinusoidal | Cholangiocyte | Periportal area |
|---|---|---|---|---|
| Donor | 11 (11/17, 64.7%)* | 0 (0/18, 0%) | 2 (2/17, 11.8%) | 1 (1/8, 12.5%) |
| Recipient | 0 (0/17, 0%) | 1 (1/18, 5.6%) | 3 (3/17, 17.6%) | 3 (3/8, 37.5%) |
| Chimera | 6 (6/17, 35.3%) | 17 (17/18, 94.4%) | 12 (12/17, 70.6%) | 4 (4/8, 50%) |
| NI† | 3 (3/20, 15%) | 2 (2/20, 10%) | 3 (3/20, 15%) | 12 (12/20, 60%) |
| Total | 20 | 20 | 20 | 20 |

LDLT, living donor liver transplantation; NI, not informative.
Four types of cell fractions were obtained from all 20 needle biopsies of LDLT grafts. Each type of sample DNA was extracted from the pool of at least three separate areas of each section.
*The % symbol indicates the fraction of respective genotypes among informative cases.

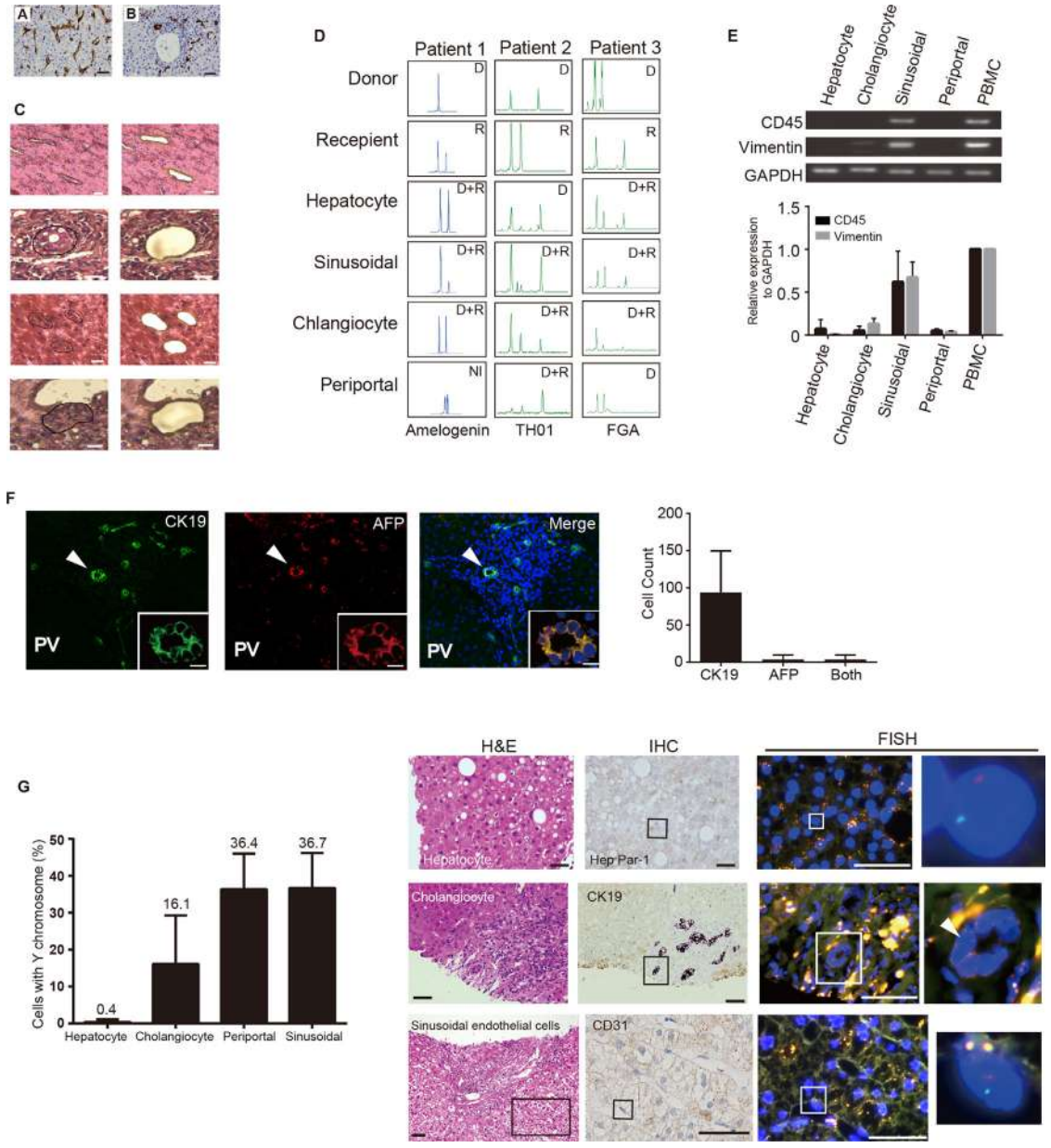


**Figure 1: Analysis of living donor liver transplantation (LDLT) biopsy specimens**. (A–C) Liver biopsy samples from 6 mo after LDLT. (A) Kupffer cells in a graft liver sinusoid stained with CD68. (B) CK7 stained bile duct epithelium from the same graft specimens. Orientation of tissue components facilitates the subsequent laser microdissection. (C) Samples before (left column) and after (right column) laser microdissection: (from the top row) sinusoidal areas, cholangiocytes, hepatocytes, and periportal areas. The purified specimens were subjected to DNA extraction. (D) Genotyping by single tandem repeat analysis of different cell populations from laser microdissection samples of a graft. A representative gene expression profile by reverse transcription–polymerase chain reaction of each laser microdissection cell type sample to evaluate the presence of hematopoietic cells and the quantitative result; CD45 and vimentin were used to detect cells of hematopoietic and nonepithelial origin, respectively. (E) GAPDH is an internal control (n = 3). (F) $CK19^{-}$ and $AFP^{+}$ cholangiocytes located close to the PV and the merged image: The entire section of needle biopsy specimens were subject to bile duct count (n = 8). Inset of each image indicates the enlarged bile duct, and the count of cholangiocytes in 27 periportal regions from eight needle biopsy samples is presented (n = 8). The histogram presents the average Y chromosome frequency of the respective cell type (n = 3), representative liver allograft H&E and IHC images, and corresponding FISH for the Y (green) and X (red) chromosome images in which each inset represents an area enlarged in the image to the right side. (G) Cell type was ultimately identified based on H&E and IHC. Scale bars = 50 μm (A–C), 20 μm (F), and 50 μm (G). Error bar indicates standard deviation (F and G). AFP, α-fetoprotein; D, donor; FISH, fluorescence *in situ* hybridization; H&E, hematoxylin and eosin; HepPar-1, hepatocyte paraffin 1; IHC, immunohistochemistry; NI, not informative; PBMC, peripheral blood mononuclear cells; PV, portal vein; R, recipient.

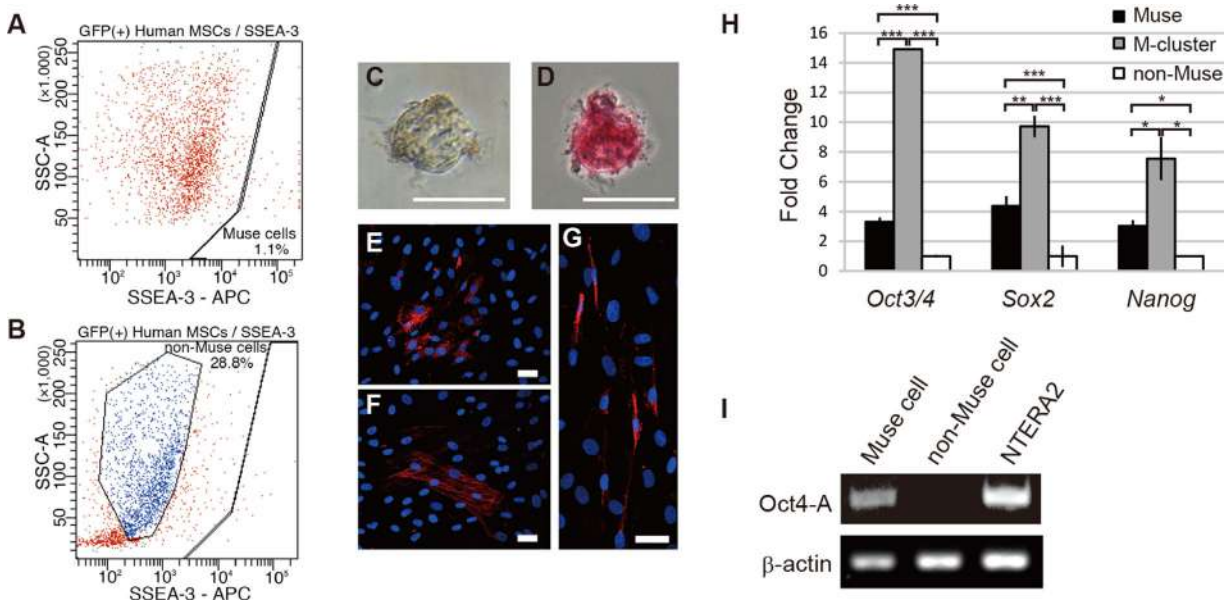


**Figure 2: Isolation of human Muse and non-Muse cells**. (A and B) Sorting of Muse and non-Muse cells from GFP-labeled h-BM-MSCs. (C) An M-cluster (i.e. Muse cell–derived clusters) (6) formed from a single Muse cell in suspension culture. (D) Alkaline phosphatase staining of an M-cluster at day 7. (E–G) Spontaneous differentiation of cells expanded from a single M-cluster on gelatin culture at day 10. Cells from the M-cluster differentiated into CK7 (E), smooth muscle actin (F), and neurofilament expressing cells (G). (H) The expression of Oct3/4, Sox2, and Nanog were analyzed in Muse, M-cluster, and non-Muse cells by quantitative reverse transcription–polymerase chain reaction. (I) Gene expression of Muse and non-Muse cells for *Oct4A* isoform. Scale bar = 100 μm. $^{*}p < 0.05$, $^{**}p < 0.01$, and $^{***}p < 0.001$. NTERA2 is a pluripotent human testicular embryonic carcinoma cell line used as a positive control. APC, allophycocyanin; GFP, green fluorescent protein; h-BM-MSC, human bone marrow mesenchymal stem cell; MSC, mesenchymal stem cell; SSEA-3, stage-specific embryonic antigen-3.

After separation, Muse and non-Muse cells were placed in a single-cell suspension culture, as described previously (6). By day 7, cell clusters—each of which was derived from a single Muse cell (M-cluster)—were formed. M-clusters were very similar to the embryoid body of human embryonic stem cells formed in suspension and were positive for alkaline phosphatase staining, which is an indicator of pluripotency (Figure 2C and 2D). We then transferred each of the M-clusters to gelatin-coated wells individually to allow the cells to expand from M-clusters for 10 days. Expanded cells exhibited spontaneous differentiation into cells that expressed CK7 ($1.55 \pm 0.34\%$, endodermal marker; biliary cells), smooth muscle actin ($3.64 \pm 1.20\%$, mesodermal marker) and neurofilament ($2.17 \pm 0.32\%$, ectodermal marker) (Figure 2E–G). In contrast, none of the non-Muse cells formed M-clusters in suspension; therefore, triploblastic-lineage marker expression was not observed. These findings are consistent with previous reports showing that a single Muse cell is able to spontaneously differentiate into cells positive for triploblastic lineage markers, whereas non-Muse cells do not exhibit these properties (6,9).

We also found that expression levels of *Oct3/4*, *Sox2*, and *Nanog* in Muse cells were higher than those in non-Muse cells and were substantially elevated when Muse cells formed M-clusters (Figure 2H). There are three isoforms of *OCT4*, namely, A, B, and B1. *OCT4A* is known to be specific for pluripotent stem cells, such as embryonic stem cells, but *B* and *B1* are also expressed in somatic cells (18). Muse cells expressed the *OCT4A* isoform, whereas non-Muse cells did not (Figure 2I).

### *Transplantation of Muse and non-Muse cells to SCID mice after PPHx*

PPHx allows us to observe both damaged and intact areas at the transection border (Figure 3A–D). The cellular infiltration of neutrophils and monocytes was detected by 48 h (Figure 3E), and by 72 h, remodeling of the bile duct was initiated at the damaged border, with small cells accumulating at the portal triad in the intact area (Figure 3F and G). By 96 h after the PPHx, new construction of sinusoids and portal triads began at the area adjacent to the injured area (Figure 3H). The remodeling of the bile duct structures was confirmed by staining for the biliary cell marker CK7 (Figure 3I and J).

At 1 week after transplantation of human Muse and non-Muse cells into the tail vein of PPHx-SCID mice, GFP$^{+}$ Muse cells were observed at the transection border, particularly in the regions adjacent to the periportal area, and these cells were round and did not appear to be committed to differentiation (Figure 4A and B). At 2 weeks, GFP$^{+}$ cells had formed bile duct–like structures at the transection border (Figure 4C) and were detected in sinusoids of the

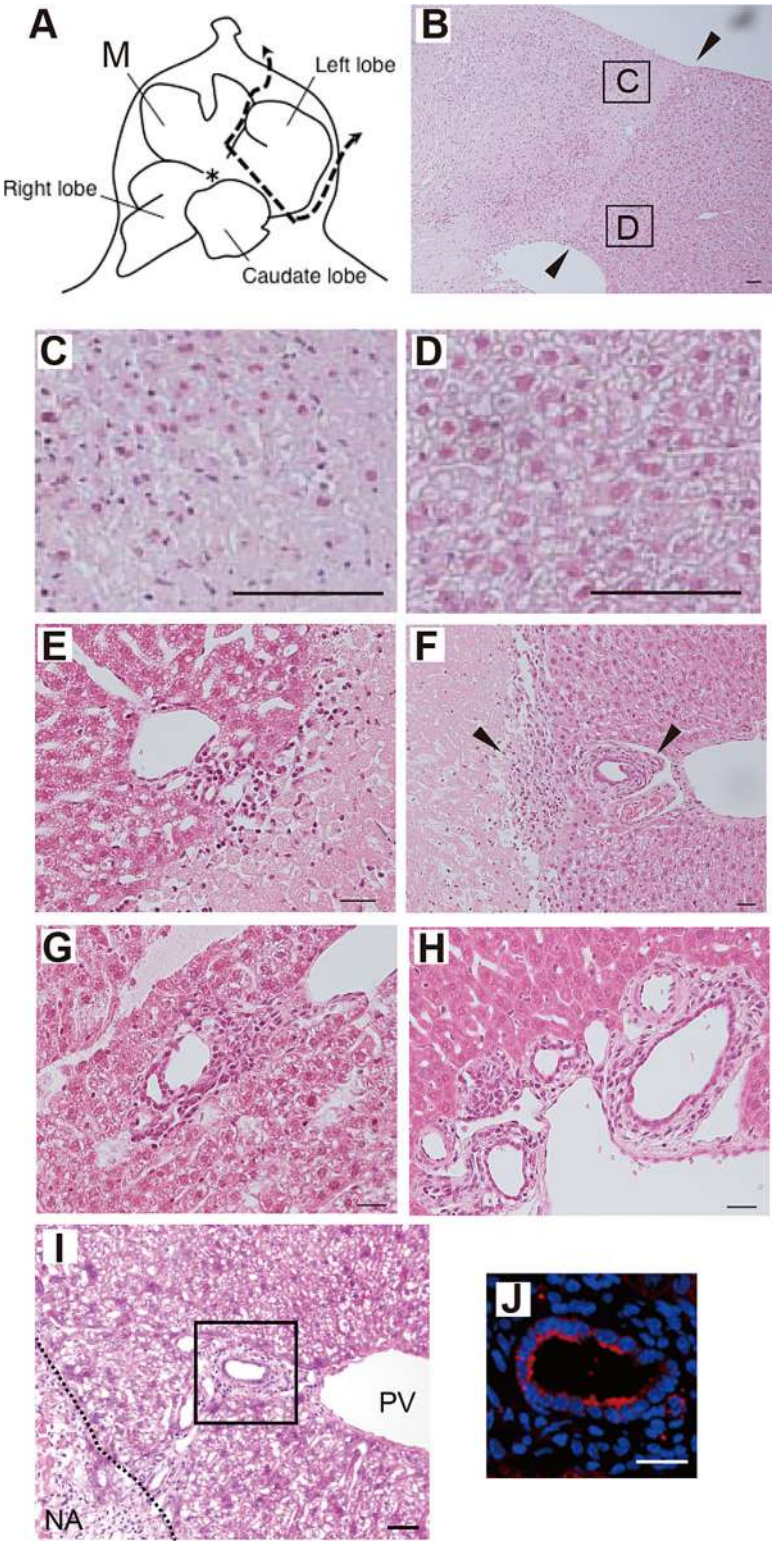


**Figure 3: Schematic of physical partial hepatectomy (PPHx) and liver section histology in the early phase after PPHx**. (A) Conventional ligation point of 2/3 PPHx (asterisk) and transected line in the left lobe in this study (arrowheads). (B–D) Transected border 24 h after PPHx (arrowheads, B). The left square is the coagulated necrosis area enlarged in (C), and the right side is the intact area (D). (E) The transected border 48 h after PPHx. (F) The border 72 h after PPHx. Small cells migrated between damaged and intact areas (left arrowhead), and bile duct remodeling was observed (right arrowhead). (G) The periportal area adjacent to the damaged site 72 h after PPHx. The bile duct remodeling continued at this time point. (H) The border 96 h after PPHx. Some vessels and bile ducts were seen as if they had constructed a portal triad. (I and J) Bile ducts and sinusoidal structures along the transected line 96 h after PPHx. Bile duct remodeling is taking place adjacent to the portal vein (I); a square area is enlarged with CK7 (red) and DAPI (blue) staining (J). Dotted line represents a border between necrotic area and healthy liver tissue. Scale bar = 50 μm. DAPI, 4′,6-diamidino-2-phenylindole; M, median lobe; NA, necrotic area; PV, portal vein.

periportal area near the transection border (Figure 4D). At 4 weeks, GFP$^+$ cholangiocyte-, hepatocyte- and sinusoid endothelial-like cells were observed at the transection border (Figure 4E–G). GFP$^+$ Muse cells were located only near the transection border and were not detected in areas distant from the transection border at any time point up to 4 weeks. In contrast, GFP$^+$ non-Muse cells were not observed anywhere in the liver at any time point

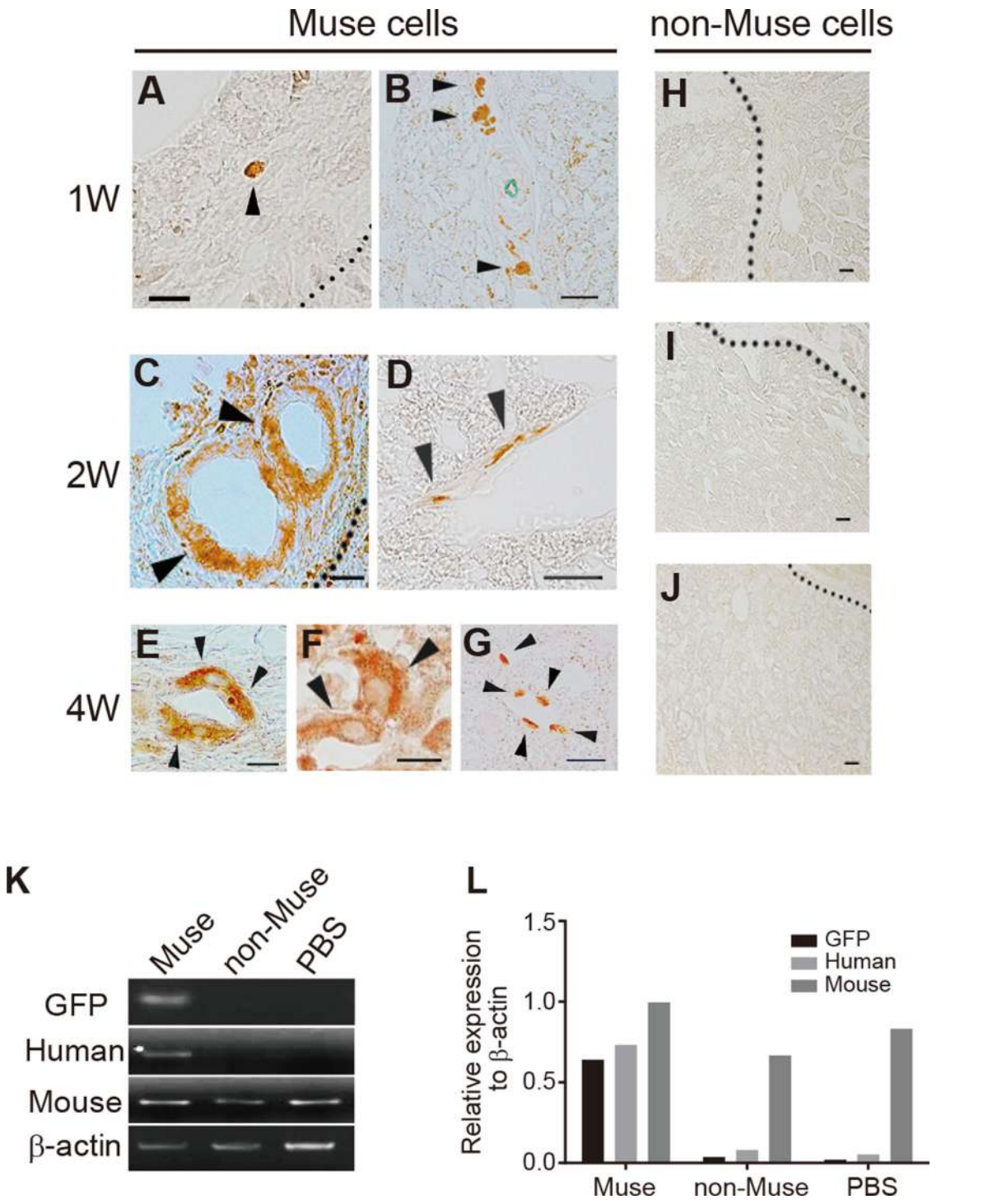


**Figure 4: Muse cell transplantation after physical partial hepatectomy**. (A–G) GFP-labeled Muse cell transplanted group. GFP-labeled cells at the transection border (A), intact periportal areas close to the transection border in which GFP$^+$ cells are occasionally seen (B), GFP$^+$ bile ducts along the transection border (C), and GFP$^+$ cells in sinusoids of the periportal area (D). (E) GFP$^+$ cells in bile duct–like structures. GFP$^+$ hepatocyte-like cells (F) and GFP$^+$ sinusoidal cells (G). (H–J) No GFP$^+$ cells were seen inside or outside (divided by dotted line) of the transection border in the non-Muse transplanted group at 1, 2, and 4 weeks. (K) To confirm that GFP$^+$ cells are derived from Muse (i.e. human origin) cells, the species-specific prostaglandin E receptor 2 gene (*PTGER2*) was assessed at 4 weeks after transplantation. (L) A gel image was quantified with β-actin as an internal control. Scale bar = 20 μm (A–J). GFP, green fluorescent protein; PBS, phosphate-buffered saline; W, weeks.

(Figure 4H–J). PBS-injected livers showed results that were similar to non-Muse cell–transplanted livers. To confirm these results, the expression of human prostaglandin E receptor 2 (*PTGER2*), mouse-specific *Ptger2* and GFP genes were assessed in liver samples at 4 weeks according to previously described methods (19). GFP genes and human *PTGER* were detected in mice that received Muse cells but not in mice that received non-Muse cells. In contrast, mouse-specific *Ptger2* was detected in both Muse cell– and non-Muse cell–injected mice (Figure 4K and L).

We next assessed the proliferative activity of Muse cells. The frequency of $Ki67^+$ cells, regardless of mouse (recipient) or human (Muse or non-Muse cells) origin, in damaged and intact areas of Muse cell–transplanted liver at day 2 after Muse cell transplantation was $11.3 \pm 1.5\%$ and $3.2 \pm 0.9\%$, respectively, and in non-Muse cell–transplanted liver was $11.2 \pm 0.7\%$ and $3.0 \pm 0.8\%$, respectively (Figure S4). At 4 weeks, the percentage of $Ki67^+$ cells in damaged and intact areas was $2.2 \pm 0.8\%$ and $1.6 \pm 0.2\%$ in Muse cell–transplanted liver, respectively, and $1.6 \pm 0.1\%$ and $1.8 \pm 0.3\%$, respectively, in non-Muse cell–transplanted liver. The frequency of $Ki67^+$ cells significantly decreased in both damaged and intact areas 4 weeks after transplantation in both groups (Student t-test, $p > 0.05$) (Figure S4). In fact, the involvement of the human transplanted cells (i.e. Muse and non-Muse cells) in proliferation seemed to be limited because the frequency of cells positive for Ki67 and human mitochondria was extremely low ($1.1 \pm 0.4\%$), even in the damaged area, suggesting that Muse cells may play different roles distinct from cellular proliferation (Figure S4).

### *Muse cells express liver progenitor cell markers after integration at an early phase*

We further investigated which lineages the $GFP^+$ Muse cells differentiated into in the early phase (2 days after transplantation) of liver tissue repair. In mice transplanted with human Muse cells, a small number of $GFP^+$ cells expressing human liver progenitor markers CK19, DLK, OV-6, and AFP were detected in the periportal area near the transection line, whereas no differentiation markers were detected (Figure 5 and Figure S5). These cells positive for GFP and liver progenitor markers were also confirmed to be positive for a human mitochondrial marker (Figure 5). In contrast, none of these markers were detected in the livers of mice transplanted with non-Muse cells or injected with PBS (data not shown).

### *Muse cells differentiate into the major liver cell types*

Liver progenitor/hepatocyte marker expression was assessed in human $GFP^+$ Muse cell–transplanted livers. At 1 week after transplantation, integrated $GFP^+$ Muse cells expressed human-specific CD19, DLK, OV6, and AFP (Figure 6), whereas mature liver component markers, such as HepPar-1, albumin, $\alpha$1-antitrypsin, CK7, and Lyve-1, could not be detected in the $GFP^+$ Muse cells (data not shown). At 2 weeks, however, these cells expressed human-specific HepPar-1, albumin, $\alpha$1-antitrypsin, CK7, and Lyve-1 (Figure 7), whereas a very small number of cells positive for liver progenitor markers were still detected. These results suggest that integrated Muse cells shifted in their differentiation toward mature cell types at 2 weeks.

At 4 weeks, $GFP^+$ Muse cells expressed human hepatocyte paraffin 1 (HepPar-1), CK7, human Lyve1, and CD68, in which 13.1% of hepatocytes ($HepPar\text{-}1^+$ cells) near the transection border were considered to be derived from $GFP^+$ Muse cells (Figure 8A). $GFP^+$ cells also expressed markers of functional hepatocytes, such as human albumin and human $\alpha$1-antitrypsin (Figure 8A). To ensure that $GFP^+$ cells were of human origin, the samples were stained for GFP and human mitochondria. Cell types that had differentiated into hepatocytes and bile duct cells were also positive for human mitochondrial markers, indicating that the $GFP^+$ cells were of human origin (Figure 8B). Moreover, staining with anti-CK7—reactive to both human and mouse—showed that $GFP^+/CK7^+$ cells, which were suggested to be derived from human Muse cells, were properly integrated into the mouse bile duct, which was primarily composed of $GFP^-/CK7^+$ mouse cholangiocytes (Figure S6). The quantitative fraction of each lineage marker–positive cell type in the integrated $GFP^+$ human Muse cells at 4 weeks is summarized in Table 2.

In contrast, no $GFP^+$ cells were detected in any tissue structure in the livers of non-Muse cell–transplanted or PBS-injected mice at any time point (data not shown). These results indicate that human Muse cells from h-BM-MSCs differentiated into the major tissue components of the liver. The marker expression profile from day 2 through 4 weeks is summarized in Table 3.

### *Fusion is unlikely to be a predominant mechanism in the differentiation of Muse cells*

At day 2, $CK19^+/GFP^+$ cells possessed only human chromosomes, whereas $CK19^+/GFP^-$ cells possessed only mouse chromosomes (Figure 9A). Cells double-positive for human and mouse chromosomes were not detected at day 2; however, at 4 weeks after transplant, the majority (98.1%; 106 of 108 cells) of $HepPar\text{-}1^+/GFP^+$ cells from mice receiving human Muse cells possessed only human chromosomes, whereas a very small number of the $HepPar\text{-}1^+/GFP^+$ cells (1.9%; 2 of 108 cells) possessed both human and mouse chromosomes (Figure 9B). No cells possessing both human and mouse chromosomes were detected among $CK7^+/GFP^+$ cells (data not shown). Consequently, the frequency of fusion between human Muse cells and host hepatocytes/cholangiocytes is extremely low, if present at all. These findings indicate that the mechanism of liver regeneration is unlikely to be largely dependent on fusion and suggest that the fusion cells do not represent a major precursor source for the differentiated cells.

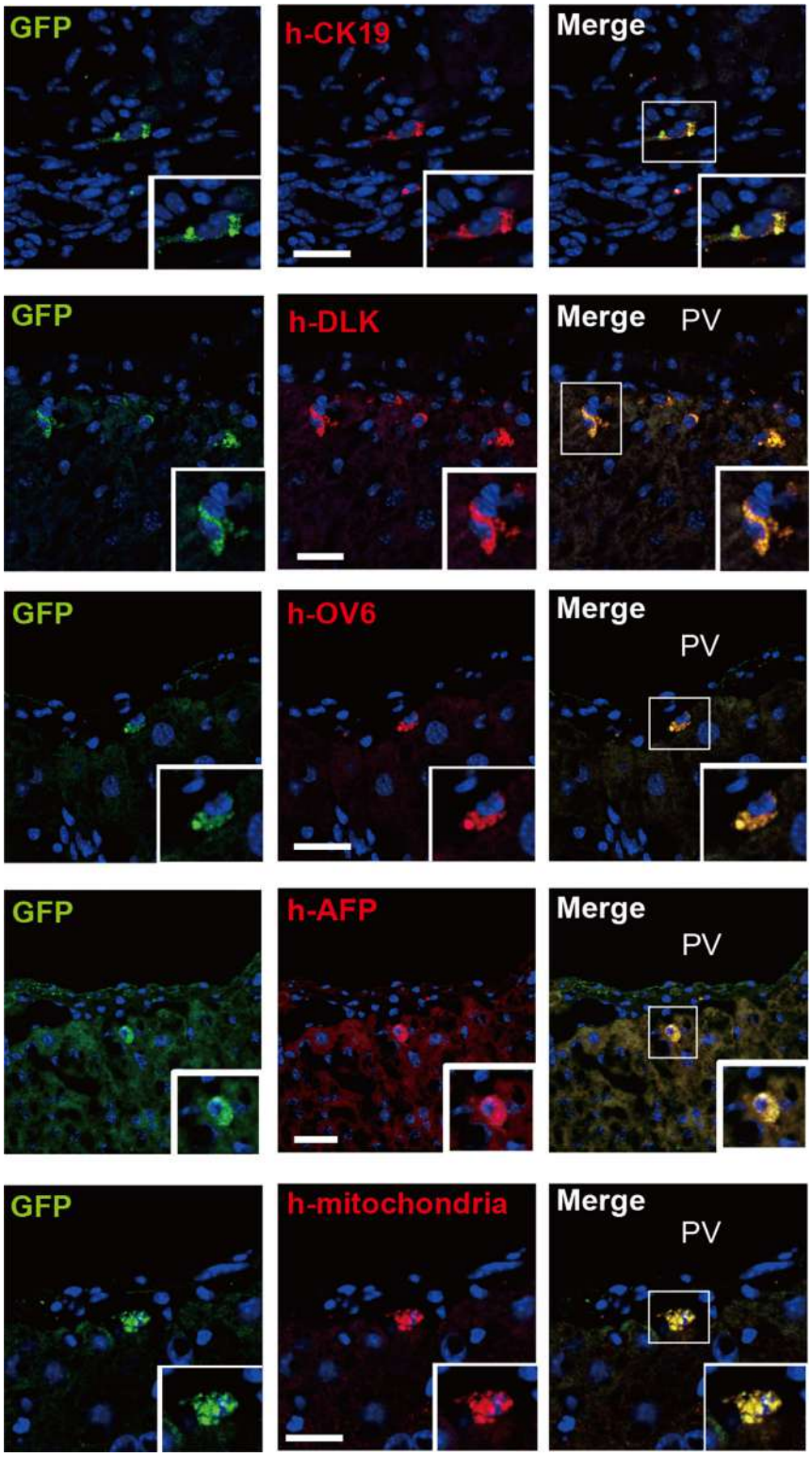


**Figure 5: Muse cell differentiation detected with human liver progenitor markers at day 2 after transplantation**. Expression of human CK19, DLK, OV-6, and AFP. Human mitochondria staining was used to confirm whether the GFP$^+$ cells were of human origin. Insets show high-power magnification of the region indicated by boxes. Scale bar = 20 μm. AFP, α-fetoprotein; GFP, green fluorescent protein; h, human; PV, portal vein.

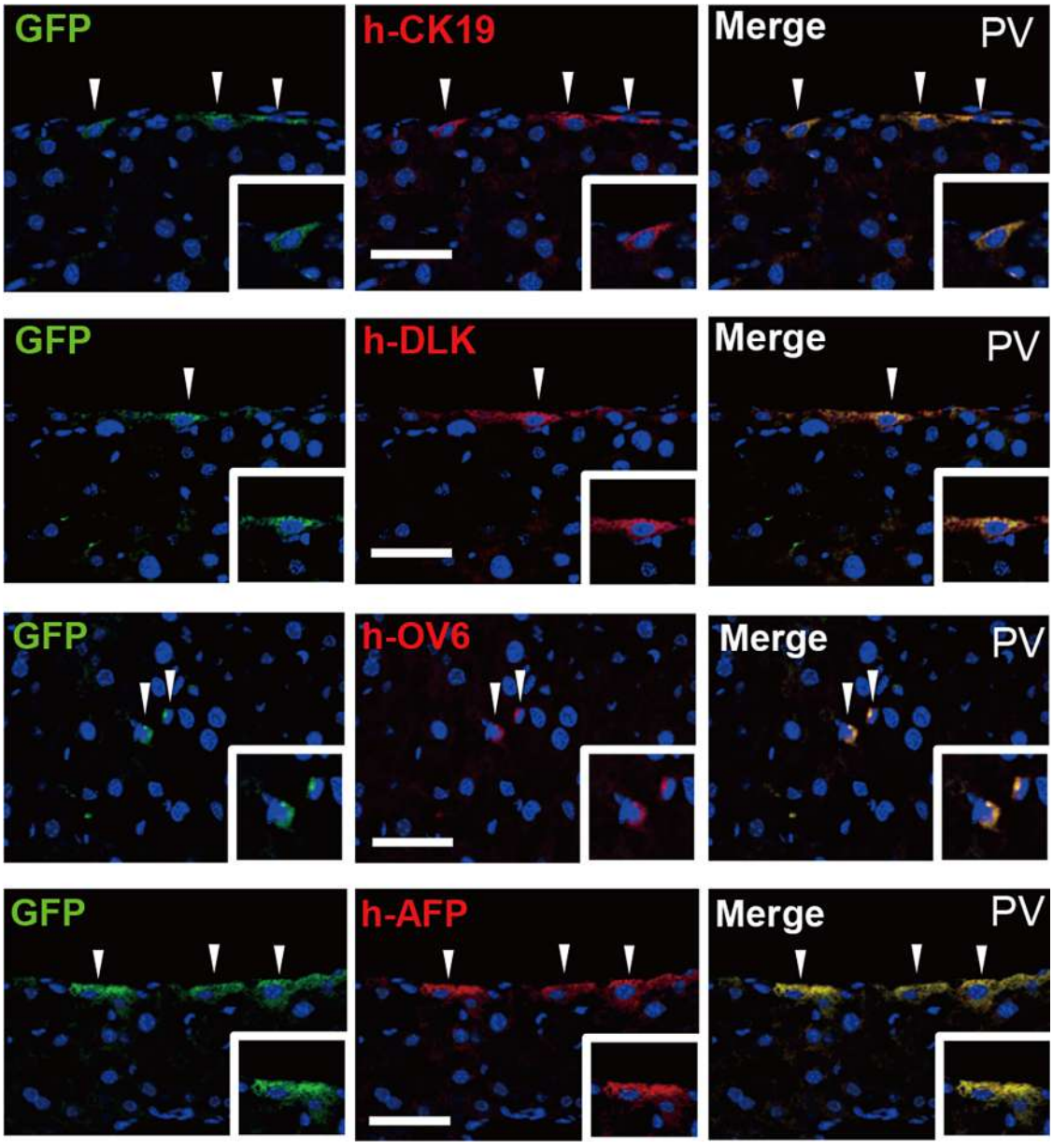


**Figure 6: Integrated Muse cell differentiation at 1 week after transplantation**. Expression of human CK19, DLK, OV-6, and AFP in integrated GFP$^+$ Muse cells at 1 week. Arrowheads indicate staining-positive cells. Insets show high-power magnification of the region indicated by boxes. Scale bar = 50 μm. AFP, α-fetoprotein; GFP, green fluorescent protein; h, human; PV, portal vein.

## Discussion

In human LDLT, we demonstrated that extrahepatic recipient cells were detectable in the graft liver as a liver component. We next assessed Muse cells as a source of extrahepatic cells, which correspond to 1–2% of total BM-MSCs. Because Muse cells (a) are able to generate cells representing all three germ layers from a single cell, (b) express pluripotency genes at a lower level than embryonic stem cells but at a higher level than non-Muse cells and (c) differentiate into cells positive for AFP and albumin at a high frequency (≈90%) under cytokine induction, they are considered to be a plausible subpopulation of BM-MSCs that effectively contribute to liver regeneration (9). We found that Muse cells injected into the tail vein of SCID mice after PPHx integrated into the regenerating region of the liver and remained there for at least 4 weeks after transplantation, whereas non-Muse cell subpopulations of BM-MSCs were not detected in the liver by either immunohistochemistry or species-specific DNA analysis up to 4 weeks after transplant. Integrated Muse cells were found to spontaneously differentiate into major

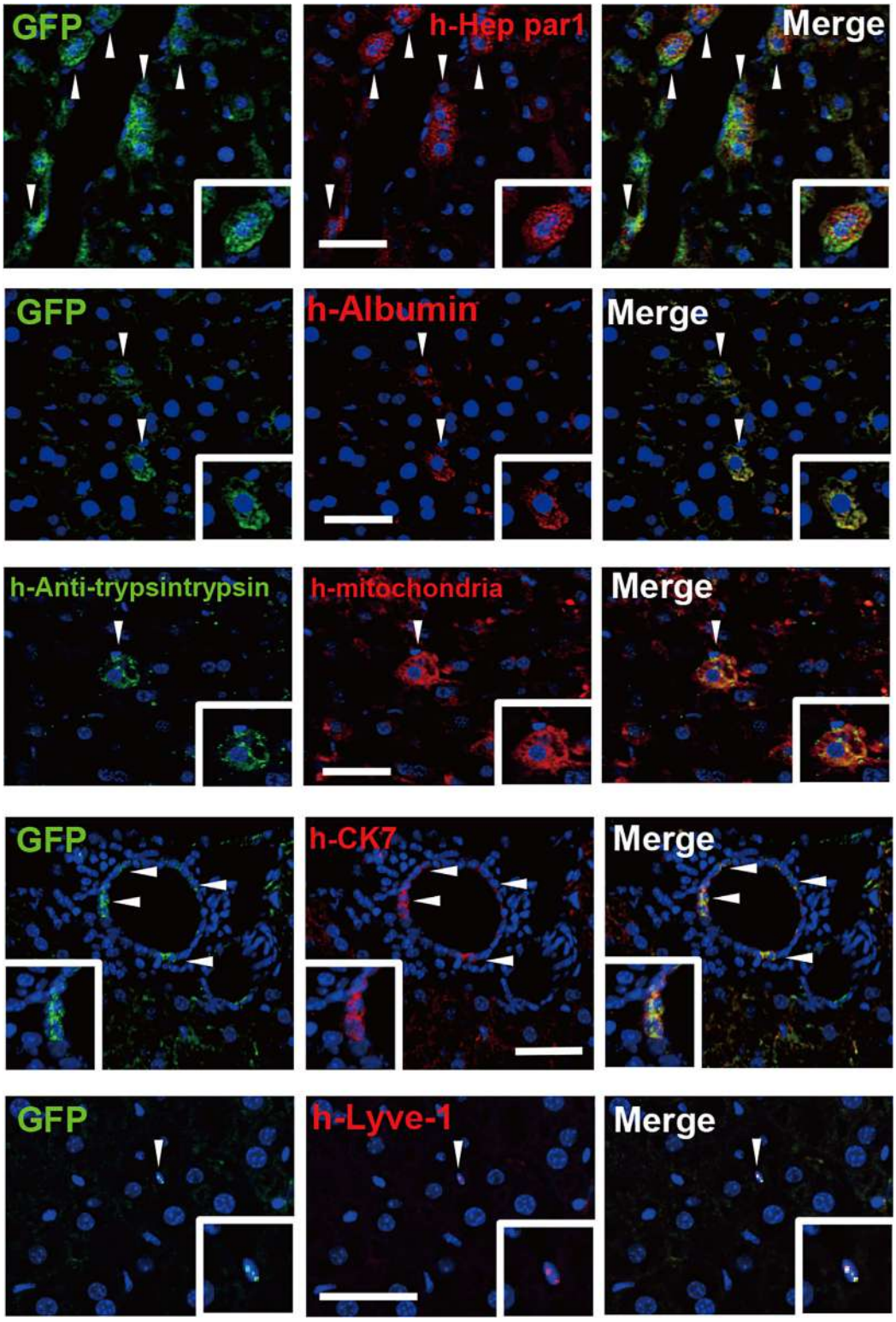


**Figure 7: Integrated Muse cell differentiation at 2 weeks after transplantation**. Expression of human HepPar-1, albumin, antitrypsin, CK7, and Lyve1 in integrated GFP$^+$ Muse cells at 2 weeks. Arrowheads indicate staining-positive cells. Insets show high-power magnification of the region indicated by boxes. Scale bar = 20 μm. GFP, green fluorescent protein; h, human; HepPar-1, hepatocyte paraffin 1.

**Table 2:** Fraction of lineage marker expressing cells in the human Muse cell transplanted group at 4 weeks

| Lineage | Marker | Fraction of lineage marker positive cells in $GFP^+$ cells (%)* |
|---|---|---|
| Hepatocyte | HepPar-1 | $74.3 \pm 5.8$ |
| Cholangiocyte | CK7 | $17.7 \pm 5.2$ |
| SEC | Lyve1 | $2.0 \pm 0.5$ |
| Kupffer cell | CD68 | $6.0 \pm 1.1$ |

$GFP^+$, green fluorescent protein positive; HepPar-1, hepatocyte paraffin 1; SEC, sinusoidal endothelial cells.
*Calculated from three views with >50 $GFP^+$ cells per view.

liver components, including hepatocytes (HepPar-1$^+$), cholangiocytes (CK19$^+$), sinusoidal endothelial cells (Lyve-1$^+$), and Kupffer cells (CD68$^+$). Muse cells also began to express the functional markers human albumin and α1-antitrypsin at 2 weeks after transplantation. Moreover, Muse cells expressed the liver progenitor markers CK19, DLK, OV-6, and AFP at 2 days after PPHx. These results suggest that after integration in the liver tissue, Muse cells first differentiate into liver progenitor cells and then subsequently into each of the liver components. The integration was particularly observed at the transection border in the Muse cell transplantation experiment, in which 13.1% of hepatocytes were found to be of Muse cell origin, whereas only 0.4% of hepatocytes were of extrahepatic origin in LDLT. In LDLT, the area close to the transection line must be avoided in biopsy for safety reasons. This limitation may have resulted in the difference in hepatocyte frequency with extrahepatic origin between the mouse model and LDLT.

During liver regeneration, the possibility of cell fusion is an important factor for consideration. The frequency of cell fusion is generally very low, ranging from 1 in $5.0 \times 10^6$ cells (20) to <1% of cells (21). In human LDLT grafts, previous FISH experiments showed that the majority of recipient-derived cells were found in liver component

**Table 3:** Hepatoblast/hepatocyte-marker expression profile at 2 days, 1 week, 2 weeks, and 4 weeks after human Muse cell transplantation

| | Marker | 2 days | 1 week | 2 week | 4 week |
|---|---|---|---|---|---|
| Liver progenitor | CK19 | + | + | − | − |
| | DLK | + | + | − | − |
| | OV-6 | + | + | − | − |
| | AFP | + | + | − | − |
| Hepatocyte | HepPar-1 | − | − | + | + |
| | Albumin | − | − | + | + |
| | α1-Antitrypsin | − | − | + | + |
| Cholangiocyte | CK7 | − | − | + | + |
| SEC | Lyve1 | − | − | + | + |
| Kupffer cell | CD68 | − | − | + | + |

AFP, α-fetoprotein; HepPar-1, hepatocyte paraffin 1; SEC, sinusoidal endothelial cells.

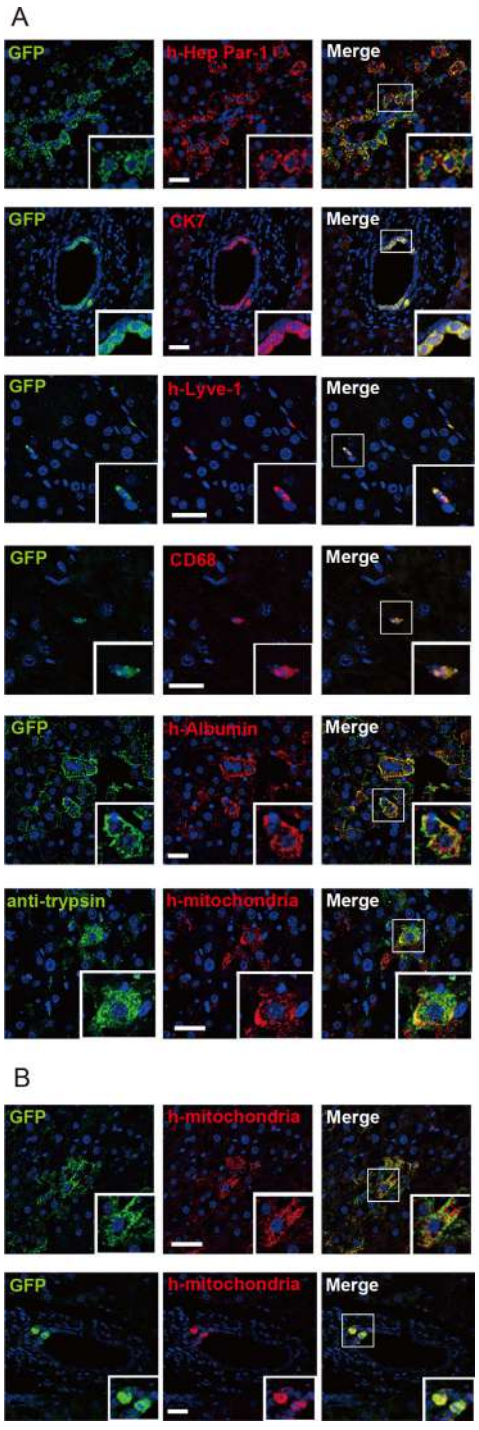


**Figure 8: Integrated Muse cell differentiation at 4 weeks after transplantation**. (A) Expression of human HepPar-1, CK7, Lyve1, CD68, albumin, and antitrypsin in integrated GFP$^+$ Muse cells at 4 weeks. (B) Human mitochondria staining was used to confirm whether the GFP$^+$ cells in hepatocytes and bile duct were of human origin. Arrowheads indicate staining-positive cells. Insets show high-power magnification of the region indicated by boxes. Scale bar = 20 μm. GFP, green fluorescent protein; h, human; HepPar-1, hepatocyte paraffin 1.

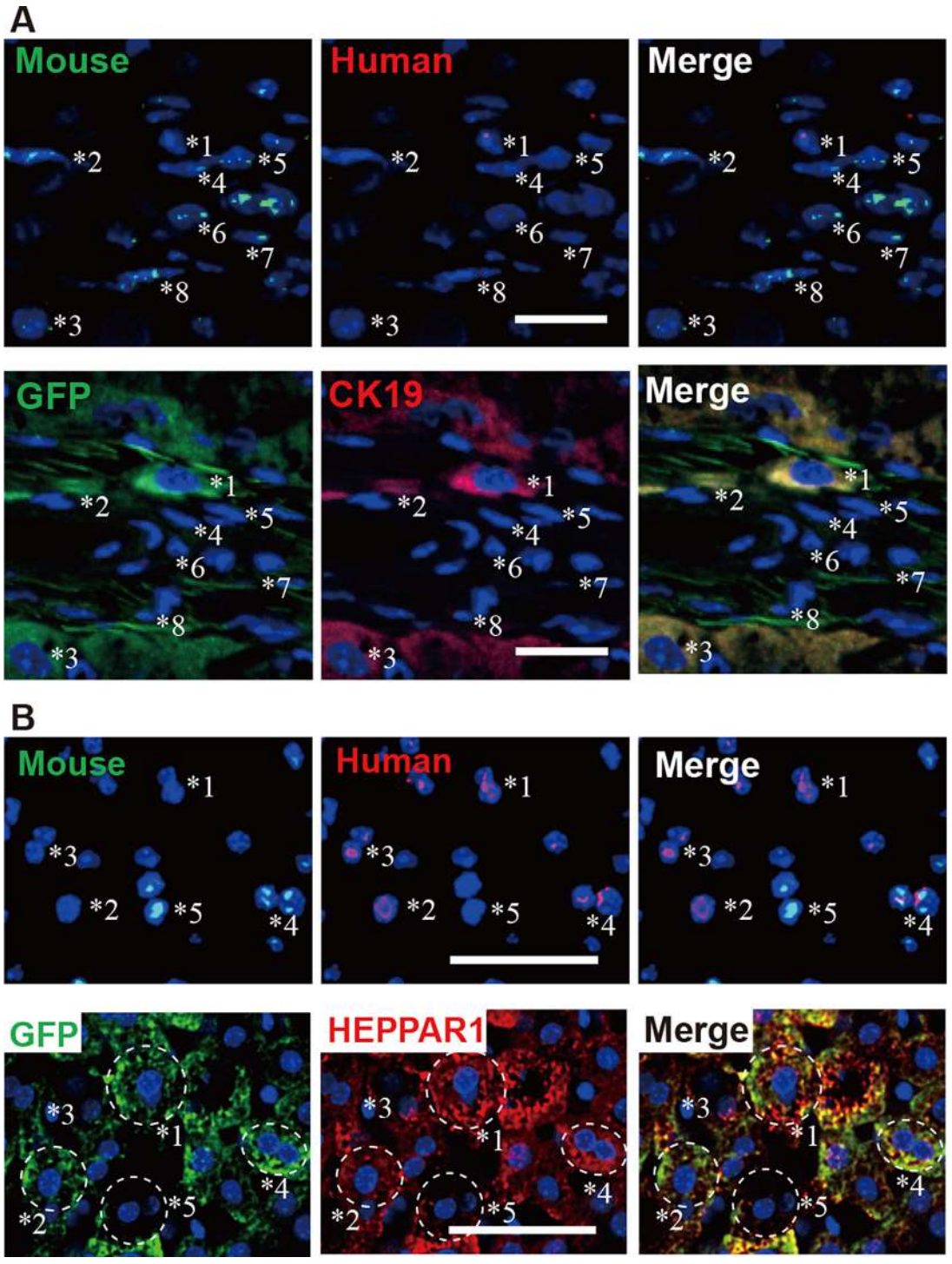


**Figure 9: FISH analysis combined with immunohistochemistry in serial sections**. At 2 days after human GFP$^+$-Muse cell transplantation, *1 cell is GFP$^+$/CK19$^+$ and possesses only human chromosomes, whereas *2–*8 cells are GFP$^-$/CK19$^-$ and possess only mouse chromosomes (A). At 4 weeks after human GFP$^+$ Muse cell transplantation, among GFP$^+$/HepPar-1$^+$ cells, *1 and *2 cells possess only human chromosomes, whereas the *4 cell possesses both human and mouse chromosomes; *3 cell that only possesses human chromosome is not reflected in the GFP/HepPar-1 section; the *5 cell is GFP$^-$/HepPar-1$^-$ and possesses only mouse chromosomes (B). Mouse and human chromosomes are indicated by green and red signals, respectively. Because the thickness of a tissue section was 8–10 μm, the nuclear location and morphology of the cytoplasm by immunohistochemistry were not exactly the same as those assessed by FISH. Scale bar = 20 μm. FISH, fluorescence *in situ* hybridization; GFP, green fluorescent protein; HepPar-1, hepatocyte paraffin 1.

structures without cell fusions (22–25), which is consistent with our current study. Our FISH and immunohistochemistry results also showed a very low frequency of human–mouse fusion cells after human Muse transplantation into our PPHx mouse model during the liver-regeneration process. Although these findings cannot immediately exclude the possibility of cell fusion during the liver-regeneration process, we concluded that cell fusion may not be the primary mechanism for hepatocyte and cholangiocyte differentiation during liver regeneration after PPHx.

Unlike artificially established cells, such as embryonic or induced pluripotent stem cells, Muse cells can be obtained from patients, donors and marrow banks with minimal manipulation (6,9). This unique characteristic minimizes ethical and tumorigenic problems. BM-MSCs can proliferate *ex vivo*, which is advantageous for producing sufficient numbers of cells for prompt clinical applications. Because BM-MSCs that were used previously in clinical studies are thought to contain a certain percentage of Muse cells (26–30), BM-derived Muse cells are likely to be a safe cellular source in a clinical setting. Nevertheless, the retention of protective cellular effects (e.g. anti-inflammatory and antiapoptosis) of soluble factors produced by BM-MSCs (8) is important because most target lesions have complex disease states. If non-Muse cells play an important role through production of trophic and anti-inflammatory factors, then their effect is not negligible, particularly in complicated pathological conditions. Nevertheless, our results demonstrate that only the Muse cell population within BM-MSCs has the capacity to differentiate into a liver component and is available without ethical issues and tumor-initiating risks (9), suggesting that the application of Muse cells for liver regeneration would be more practical than other stem cell sources (31–34). In fact, Heneidi et al recently reported that Muse cells isolated from human adipose tissue were able to differentiate into liver cells (35).

In summary, we suggest that Muse cells integrate into the regenerating area as liver progenitor cells during the early phase of the process and subsequently differentiate spontaneously into major liver components, including hepatocytes. In contrast, none of the non-Muse cells exhibited an ability to differentiate.

## Acknowledgments

The authors appreciate the excellent support provided by Yuji Suzuki and Yasuhiro Takikawa for helpful discussions, Yukiko Igawa and Chinami Onuma for work on the fluorescence *in situ* hybridization experiments and Noriyuki Yamada for preparation of pathological sections. This work was supported as a Medical Innovation by Advanced Science and Technology (MIAST) project of the Ministry of Education, Culture, Science and Technology, Japan (S1001001 to S.S.N.), and a Grant-in-Aid for Scientific Research (C) 25461959 (M. Dezawa and S. S. Nishizuka).

## Disclosure

The authors of this manuscript have no conflicts of interest to disclose as described by the *American Journal of Transplantation*.

## References

1. Aurich I, Mueller LP, Aurich H, et al. Functional integration of hepatocytes derived from human mesenchymal stem cells into mouse livers. Gut 2007; 56: 405–415.
2. Forbes SJ, Newsome PN. New horizons for stem cell therapy in liver disease. J Hepatol 2012; 56: 496–499.
3. Chamberlain G, Fox J, Ashton B, Middleton J. Concise review: Mesenchymal stem cells: Their phenotype, differentiation capacity, immunological features, and potential for homing. Stem Cells 2007; 25: 2739–2749.
4. Pontikoglou C, Deschaseaux F, Sensebe L, Papadaki HA. Bone marrow mesenchymal stem cells: Biological properties and their role in hematopoiesis and hematopoietic stem cell transplantation. Stem Cell Rev 2011; 7: 569–589.
5. Preisegger KH, Factor VM, Fuchsbichler A, Stumptner C, Denk H, Thorgeirsson SS. Atypical ductular proliferation and its inhibition by transforming growth factor beta1 in the 3,5-diethoxycarbonyl-1,4-dihydrocollidine mouse model for chronic alcoholic liver disease. Lab Invest 1999; 79: 103–109.
6. Kuroda Y, Kitada M, Wakao S, et al. Unique multipotent cells in adult human mesenchymal cell populations. Proc Natl Acad Sci U S A 2010; 107: 8639–8643.
7. Iwamoto T, Terai S, Hisanaga T, et al. Bone-marrow-derived cells cultured in serum-free medium reduce liver fibrosis and improve liver function in carbon-tetrachloride-treated cirrhotic mice. Cell Tissue Res 2013; 351: 487–495.
8. Shi C. Recent progress toward understanding the physiological function of bone marrow mesenchymal stem cells. Immunology 2012; 136: 133–138.
9. Wakao S, Kitada M, Kuroda Y, et al. Multilineage-differentiating stress-enduring (Muse) cells are a primary source of induced pluripotent stem cells in human fibroblasts. Proc Natl Acad Sci U S A 2011; 108: 9875–9880.
10. Kinoshita K, Kuno S, Ishimine H, et al. Therapeutic potential of adipose-derived SSEA-3-positive Muse cells for treating diabetic skin ulcers. Stem Cells Transl Med 2015; 4: 146–155.
11. Uchida H, Morita T, Niizuma K, et al. Transplantation of unique subpopulation of fibroblasts, muse cells, ameliorates experimental stroke possibly via robust neuronal differentiation. Stem Cells 2015 (in press)
12. Yamauchi T, Kuroda Y, Morita T, et al. Therapeutic effects of human multilineage-differentiating stress enduring (MUSE) cell transplantation into infarct brain of mice. PLoS One 2015; 10: e0116009.
13. Dezawa M, Kanno H, Hoshino M, et al. Specific induction of neuronal cells from bone marrow stromal cells and application for autologous transplantation. J Clin Invest 2004; 113: 1701–1710.
14. Wakao S, Kitada M, Dezawa M. The elite and stochastic model for iPS cell generation: multilineage-differentiating stress enduring (Muse) cells are readily reprogrammable into iPS cells. Cytometry A 2013; 83: 18–26.
15. Pittenger MF, Mackay AM, Beck SC, et al. Multilineage potential of adult human mesenchymal stem cells. Science 1999; 284: 143–147.

16. Kung C, Pingel JT, Heikinheimo M, et al. Mutations in the tyrosine phosphatase CD45 gene in a child with severe combined immunodeficiency disease. Nat Med 2000; 6: 343–345.
17. Saito T, Deskin RW, Casola A, et al. Respiratory syncytial virus induces selective production of the chemokine RANTES by upper airway epithelial cells. J Infect Dis 1997; 175: 497–504.
18. Atlasi Y, Mowla SJ, Ziaee SA, Gokhale PJ, Andrews PW. OCT4 spliced variants are differentially expressed in human pluripotent and nonpluripotent cells. Stem Cells 2008; 26: 3068–3074.
19. Alcoser SY, Kimmel DJ, Borgel SD, Carter JP, Dougherty KM, Hollingshead MG. Real-time PCR-based assay to quantify the relative amount of human and mouse tissue present in tumor xenografts. BMC Biotechnol 2011; 11: 124.
20. Terada N, Hamazaki T, Oka M, et al. Bone marrow cells adopt the phenotype of other cells by spontaneous cell fusion. Nature 2002; 416: 542–545.
21. Wang X, Willenbring H, Akkari Y, et al. Cell fusion is the principal source of bone-marrow-derived hepatocytes. Nature 2003; 422: 897–901.
22. Harris RG, Herzog EL, Bruscia EM, Grove JE, Van Arnam JS, Krause DS. Lack of a fusion requirement for development of bone marrow-derived epithelia. Science 2004; 305: 90–93.
23. Jang YY, Collector MI, Baylin SB, Diehl AM, Sharkis SJ. Hematopoietic stem cells convert into liver cells within days without fusion. Nat Cell Biol 2004; 6: 532–539.
24. Jang YY, Sharkis SJ. Metamorphosis from bone marrow derived primitive stem cells to functional liver cells. Cell Cycle. 2004; 3: 980–982.
25. Sato Y, Araki H, Kato J, et al. Human mesenchymal stem cells xenografted directly to rat liver are differentiated into human hepatocytes without fusion. Blood 2005; 106: 756–763.
26. Connick P, Kolappan M, Crawley C, et al. Autologous mesenchymal stem cells for the treatment of secondary progressive multiple sclerosis: An open-label phase 2a proof-of-concept study. Lancet Neurol 2012; 11: 150–156.
27. Hare JM, Fishman JE, Gerstenblith G, et al. Comparison of allogeneic vs autologous bone marrow-derived mesenchymal stem cells delivered by transendocardial injection in patients with ischemic cardiomyopathy: The POSEIDON randomized trial. JAMA 2012; 308: 2369–2379.
28. Le Blanc K, Frassoni F, Ball L, et al. Mesenchymal stem cells for treatment of steroid-resistant, severe, acute graft-versus-host disease: A phase II study. Lancet 2008; 371: 1579–1586.
29. Reinders ME, de Fijter JW, Roelofs H, et al. Autologous bone marrow-derived mesenchymal stromal cells for the treatment of allograft rejection after renal transplantation: Results of a phase I study. Stem Cells Transl Med 2013; 2: 107–111.
30. Yin F, Battiwalla M, Ito S, et al. Bone marrow mesenchymal stromal cells to treat tissue damage in allogeneic stem cell transplant recipients: Correlation of biological markers with clinical responses. Stem Cells 2014; 32: 1278–1288.
31. Espejel S, Roll GR, McLaughlin KJ, et al. Induced pluripotent stem cell-derived hepatocytes have the functional and proliferative capabilities needed for liver regeneration in mice. J Clin Invest 2010; 120: 3120–3126.
32. Haridass D, Yuan Q, Becker PD, et al. Repopulation efficiencies of adult hepatocytes, fetal liver progenitor cells, and embryonic stem cell-derived hepatic cells in albumin-promoter-enhancer urokinase-type plasminogen activator mice. Am J Pathol 2009; 175: 1483–1492.
33. Ishikawa T, Banas A, Teratani T, Iwaguro H, Ochiya T. Regenerative cells for transplantation in hepatic failure. Cell Transplant 2012; 21: 387–399.
34. Wakitani S, Okabe T, Horibe S, et al. Safety of autologous bone marrow-derived mesenchymal stem cell transplantation for cartilage repair in 41 patients with 45 joints followed for up to 11 years and 5 months. J Tissue Eng Regen Med 2011; 5: 146–150.
35. Heneidi S, Simerman AA, Keller E, et al. Awakened by cellular stress: Isolation and characterization of a novel population of pluripotent stem cells derived from human adipose tissue. PLoS One 2013; 8: e 64752.

## Supporting Information

Additional Supporting Information may be found in the online version of this article.

**Figure S1: Schematic representation of living donor liver transplantation (LDLT)**. LDLT is a surgical procedure in which a living donor undergoes physical partial hepatectomy. The transected liver is then transplanted into a recipient body.

**Figure S2: Positive and negative controls for CK19 and α-fetoprotein (AFP) immunostaining**. An anti-CK19 antibody was used to stain an intact human liver section for the detection of cholangiocytes. An anti-AFP antibody was used to stain a human hepatocellular carcinoma (all tumor cells are positive in the cytoplasm).

**Figure S3: Single tandem repeat analysis for all five loci**. *, non-Donor allele. D, donor; NI, not informative; R, recipient.

**Figure S4: Hepatocyte proliferation in the damaged area of the liver**. Ki67 immunostaining and DAPI (4′,6-diamidino-2-phenylindole) staining on the marginal zone of the liver at day 2 (A) and 4 weeks (B) after cellular transplantation. The average frequency and standard error of Ki67+ cells is indicated in the respective conditions. Ki67+ cells among human mitochondria–positive cells at 4 weeks after cellular transplantation (C). The frequency was calculated from multiple views containing at least 600 cells per view. *Damaged area in (A). Bar = 50 μm.

**Figure S5: Low-power view of a mouse liver sample used for immunohistochemistry of human liver progenitor markers after Muse cell transplantation**. The area of the inset is ≈4 mm away from the transection line (dotted line).

**Figure S6: Immunostaining of a Muse cell transplanted liver (4 weeks)**. An anti-CK7 antibody reacts with both

mouse and human CK7. GFP+/CK7+ cells suggested Muse-derived cells integrated into the mouse bile duct, which also included GFP−/CK7+ mouse cholangiocytes.

**Table S1:** Primer sequences used for human samples.

**Table S2:** List of antibodies used for immunohistochemistry.

**Table S3:** Clinical characteristics of living donor liver transplantation cases.

**Table S4:** The numbers of cells with recipient origin Y chromosomes in each cell type.

**Table S5:** Average frequency of recipient origin in each cell type.